Heat and Mass Transfer (2022) 58:1381–1391
https://doi.org/10.1007/s00231-022-03190-6

ORIGINAL ARTICLE

Thermoelectric investigation of low-cost modular night-time electricity generation

Shahvaiz Khan[1] · Taqi Ahmad Cheema[1] · Malik Hassan[1] · Muhammad Sohail Malik[1] · Cheol Woo Park[2]

Received: 10 September 2021 / Accepted: 16 February 2022 / Published online: 23 February 2022

Abstract

One of the major pressing issues in today's world is meeting the ever-increasing demand for sustainable and environment-friendly energy. To address this issue, renewable systems that capture energy through diverse energy scavenging techniques and devices are gaining interest. Among the aforementioned devices, thermoelectric generators (TEGs) are the temperature-dependent electricity-producing component that converts the temperature gradient (thermal input) directly into electrical energy without negatively affecting the environment. In the present study, a TEG was used to generate electricity using the radiative night-time sky cooling phenomenon. Both experimental and numerical approaches were applied to investigate the morphological characteristics of TEGs for night-time electricity generation. An in-house built night-time TEG model consisting of top and bottom plates, a block, and a TEG module sandwiched between them was used in this study. The effect of morphological characteristics, such as the type of material (Aluminium and Copper), the plate thicknesses, the number of thermocouples and the TEG leg length, on the open-circuit voltage was investigated. Experimental and numerical simulation results were found to be qualitatively consistent. Moreover, the reduction in plate thickness, the increase in the number of thermocouples, and the increase in TEG leg height increased the open-circuit voltage. The proposed model can act as a base model for the design and development of future models for night-time electricity generation.

1 Introduction

Currently, 1.3 billion individuals worldwide do not have consistent access to electricity, primarily in developing nations [1]. Moreover, the rapid industrial development and world population growth pose a serious threat to worldwide energy resources, leading to an increase in global warming [2–4]. Fossil fuels are presently the most familiar energy assets being utilised for power generation. Meanwhile, solar, wind and hydro energy are the renewable energy resources widely used for electricity generation [5–10]. Except for solar energy, all these resources are expensive. However, most of the sun's radiations collected by a photovoltaic (PV) panel are dissipated as heat and a solar conversion efficiency of only 10% to 20% is achievable in practical applications [11, 12]. Furthermore, the distribution of solar energy around the globe is non-uniform, depriving some regions of PV energy for months [13]. In addition, solar panels can only operate efficiently during the day; thus, night-time consumers of electricity are dependent on storage devices that are attached to PV plates. Developing an off-grid electricity generator that can generate electricity at night-time is a viable approach to this problem. In this regard, researchers have employed radiative cooling phenomenon in combination with thermoelectric generators (TEGs) for night-time electricity generation. In the future, this approach will not only benefit the people living in remote regions but also help in off-grid electricity generation, like in traffic signal lightning [14]. Moreover, TEGs can be coupled with solar panels to increase their efficiency [15].

TEG is a thermoelectric device that uses the Seebeck effect to convert the temperature gradient effectively into electrical output [16]. The Seebeck effect is a type of thermoelectric effect in which voltage is produced by the temperature difference [17]. TEGs are made up of P-type and

✉ Taqi Ahmad Cheema
tacheema@giki.edu.pk

✉ Cheol Woo Park
chwoopark@knu.ac.kr

[1] Faculty of Mechanical Engineering, GIK Institute of Engineering Sciences and Technology, Swabi 23460, Pakistan

[2] School of Mechanical Engineering, Kyungpook National University, 80 Daehak-Ro, Buk-Gu, Daegu 41566, South Korea

N-type semiconductors with a heat sink and a heat source on each side [18–20]. Furthermore, the temperature difference across a TEG can be obtained by either lessening the cold side's temperature or elevating the hot side's temperature or simultaneously adjusting both. Consequently, thermal management of TEG's cold side is also important for maintaining enough temperature difference [21–25].

In radiative sky cooling, an object on earth is cooled by the emission of thermal radiations to the cold atmosphere through an air window with a wavelength range of 8–13 μm [26]. Materials that can absorb energy and emit it in the afore-mentioned wavelength display a cooling phenomenon. Moreover, materials that can reflect 95% of the sunlight exhibit cooling even in direct sunlight [27]. According to a recent discovery, a silicon photodiode undergoes radiative interchange with a cool surface and generates electricity by scavenging the diode's outgoing thermal radiation [28–31]. Moreover, daytime radiative sky cooling has also received great interests globally [32, 33]. On the basis of the radiative sky cooling concept, the first piece of work related to night-time electricity generation was published by Raman et al. [1]. They experimentally developed a basic and cost-effective method for obtaining energy at night through a TEG that produces sufficient energy to power a light-emitting diode without any active power input. Later, they made improvements in their setup to enhance the power output. For this purpose, the emissivity spectra, the figure of merit (a term used to describe the system's performance, process, or equipment relative to its alternatives) and thermal convection were improved, and the ratio of areas between

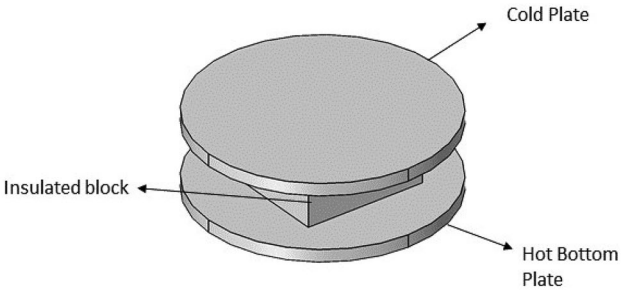

Fig. 1 3D model of night-time TEG used in the present study

the TEG and the radiative cooler was adjusted, resulting in a power density increase of 153% [13]. Moreover, Ishii et al. developed a model that generated electricity during the day and at night using radiative cooling [34]. The model's core purpose was to generate electricity without dropping the electric potential to zero in 24 h. To achieve that goal, two models were developed. One model had a selective emitter (SE) surface that comprised a 100-nm thick aluminium film mounted on the bottom of a glass. The other had a black emitter surface with a layer of black paint on a glass's top side. The SE surface resulted in the generation of electricity during the day and at night without falling to zero within 24 h, whereas the black emitter resulted in the generation of electricity during the day and at night, but its value dropped to zero multiple times.

The literature clearly indicates that most of the studies involving night-time electricity generation are experimental and theoretical works. However, the potential in this area

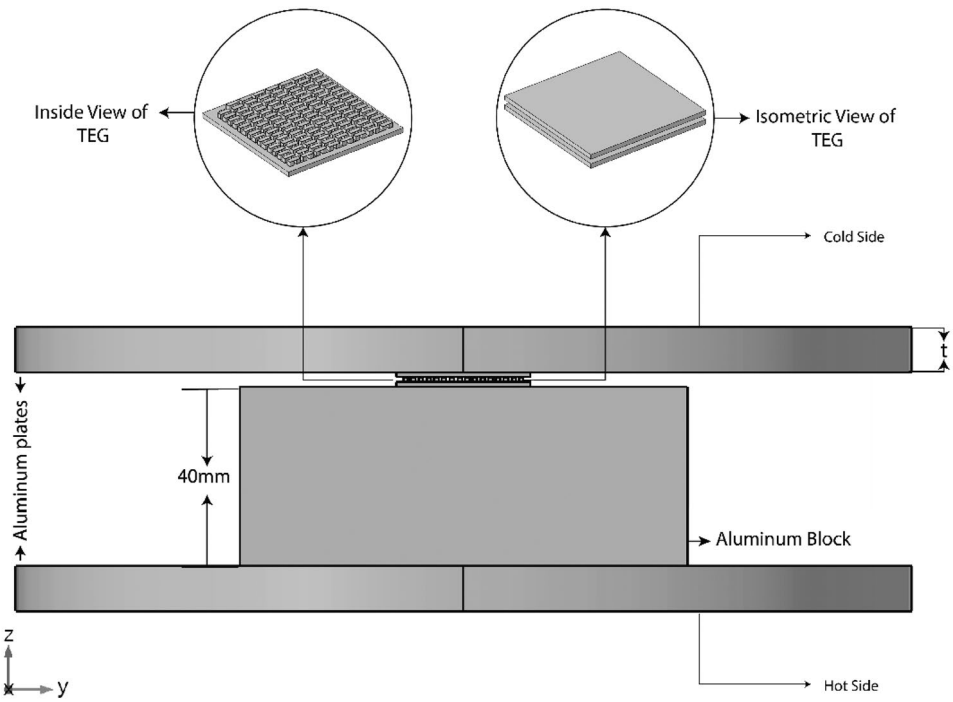

Fig. 2 Detailed view of the night-time TEG model used in the present study

Table 1 Characteristics of TEGs

Parameters	Length of TEG (mm)	Width of TEG (mm)	Height of TEG (mm)	Leg length (mm)	Leg width (mm)	Leg height (mm)	Number of Thermocouples inside TEG
Values	40	40	3.8	1	1	1	127

has not been fully explored. In this regard, the authors of the present study identified a research gap that requires the use of numerical simulation. Given the advantage of numerical simulation over experimental studies in terms of forecasting the physical phenomenon, the performance of experimental and numerical models must be elucidated, and the parameter distributions should be visualised with improved and cost-effective designs. Moreover, simulations can provide an approximate solution when an analytical solution is impossible, and the system's future can also be predicted.

Inspired by the experimental study of Raman et al., the present study aims to develop and investigate a numerical model of night-time TEG and validate it using an in-house developed experimental setup [1]. After validation with the experimental results, the proposed model can act as a base model for the design and development of future models for night-time electricity generation. The potential of this model lies in its ability to provide a clear comparison between the maximum open-circuit voltage achieved through experimentation and the maximum electric potential achieved through the numerical model. Moreover, improvements can be made by investigating the material and design modifications. Furthermore, by just changing a few parameters, the model can work for other commercially available TEGs.

2 Model description

The schematic representation of the night-time TEG model consisting of aluminium plates, an aluminium block, and a TEG is shown in Fig. 1. Similarly, the inside view of the TEG is shown in Fig. 2. The TEG modelled in the present study uses the geometric dimensions and features of the actual TEC1-12706 model as given in Table 1. Table 2 lists the temperature-dependent thermo-physical properties of the same TEG. The temperature differences are applied at the top and bottom plates with a maximum value of 2.5 K. The material properties of the aluminium and copper used in the night-time TEG are also shown in Table 2. Moreover, the thermocouples in the TEG are electrically connected in series while thermally in parallel as shown in Fig. 3. In the proposed model, the plate on the upper side is the cold plate, while the plate on the lower side is the hot plate. Thus, the temperature differential is set up between the plates, and voltage is produced.

3 Mathematical model and governing equations

The numerical model assumes the following:

a. A steady-state 3D model
b. Negligible internal, thermal and electric contact resistances
c. Heat is solely transferred by conduction because the thermoelectric domains are insulated

3.1 Governing equations

Given that the thermoelectric effect is a Multiphysics study of the thermal and electric effect, the equations of both effects are employed.

i. Heat transfer modelling

For the steady state, the energy balance in the three domains is governed by Eq. (1). The first and second terms on the left side of the equation represent the rates of convection heat transfer and conduction transfer, respectively. The first term at the right side of the equation is the heat source or sink term, and thermoelastic damping is shown in the second term.

$$\rho C_p u \nabla T + \nabla .q = Q + Q_{Ted}, \quad (1)$$

where ρ represents the density, C_p denotes the heat capacity, and ∇T denotes the temperature gradient. Moreover, conduction heat transfer rate q is given by the well-known Fourier's law of heat conduction

Table 2 Material properties of Copper and Aluminium

Material Property	Electrical conductivity [S/m]	Resistivity (Ω-cm)	Thermal conductivity [W/(m–K)]	Coefficient of thermal expansion [1/K]
Copper	6×10^{7}	1.72×10^{-8}	400	1.7×10^{-5}
Aluminium	3.77×10^{7}	2.65×10^{-8}	238	23×10^{-6}

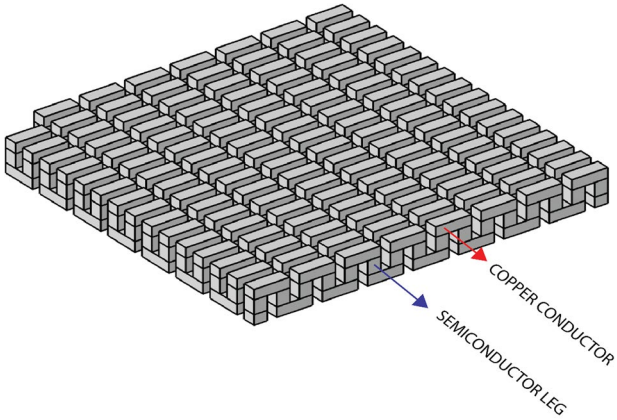

Fig. 3 Thermopile inside a thermoelectric generator

$$q = -kA\frac{dT}{dx}, \tag{2}$$

where k is the thermal conductivity of the material, A represents the area through which heat passes, dT is the temperature difference and dx represents the thickness.

ii. Electric current modelling

According to the law of conservation of charge, the electric charge in an isolated system remains constant. The Eq. (3) is used for charge conservation for a stationary case for the finite element analysis of the model.

$$\nabla.J = Q_{j,v}, \tag{3}$$

where $Q_{j,v}$ represents charge source; J represents the current density and is derived using Eq. (4) in which J_e denotes an external current source and σE represents the conduction current with electrical conductivity σ.

$$J = \sigma E + J_e, \tag{4}$$

where E denotes the electric field which is derived using Eq. (5), ∇V represents the potential difference, and negative sign indicates that the vectors representing the electric fields point in the direction of decreasing electric potential.

$$E = -\nabla V, \tag{5}$$

3.2 Data reduction

Heat transfer is considered to occur through conduction only. Thus, heat transfer by convection, heat source or sink and thermo-elastic damping is considered to be zero. Hence, Eq. (1) becomes

$$\nabla.q = 0, \tag{6}$$

Moreover, no source of charge is attached. Thus,$Q_{j,v} = 0$, so Eq. (3) can be rewritten as

$$\nabla.J = 0, \tag{7}$$

Furthermore, no current source is attached. Thus, $J_e = 0$, and Eq. (4) becomes

$$J = \sigma E, \tag{8}$$

4 Thermal model

The thermal model of a unit thermocouple for night-time electricity generation is presented in Fig. 4 in the form of thermal domains. The thermal resistances represented in Fig. 4b are connected in series and parallel combinations. In Fig. 4b, R1, R2, R3, R4, R5, R6, R7, R8, R9, and R10 denote thermal resistances of the top cold plate, the ceramic on the top side, the copper conductor, the N-type semiconductor, the P-type semiconductor, the N-type side copper conductor, the P-type side copper conductor, the bottom ceramic plate, the insulated block, and the hot bottom side, respectively. Equation (2) can also be written as

$$q = \left(T_h - T_c\right)/R, \tag{9}$$

where, T_h represents the temperature of the hot plate (hot bottom side), T_c represents the temperature of the cold plate (cold top plate), and R is given as

$$R = R1 + R2 + R3 + \frac{(R4 + R6)(R5 + R7)}{R4 + R5 + R6 + R7} + R8 + R9 + R10, \tag{10}$$

In the present model, the Dirichlet boundary condition is applied with a fixed value of temperatures in different cases on the top and bottom surfaces of the plates. Moreover, one of the surfaces of the copper conductor was grounded, while the aluminium block was insulated to have as much temperature difference between the top and bottom domains as possible.

5 Mesh independence

The results of mesh independence analysis for three different plate thicknesses and the finally used three-dimensional mesh across the computational domains are displayed in Figs. 5 and 6. Tetrahedral elements were used to divide the heat flow domains. After the element selection, its sensitivity was examined for different grid sizes for three different models with different top and bottom thicknesses as shown in Tables 3, 4 and 5. The value of open-circuit voltage which is also a reference in the present study is analyzed at

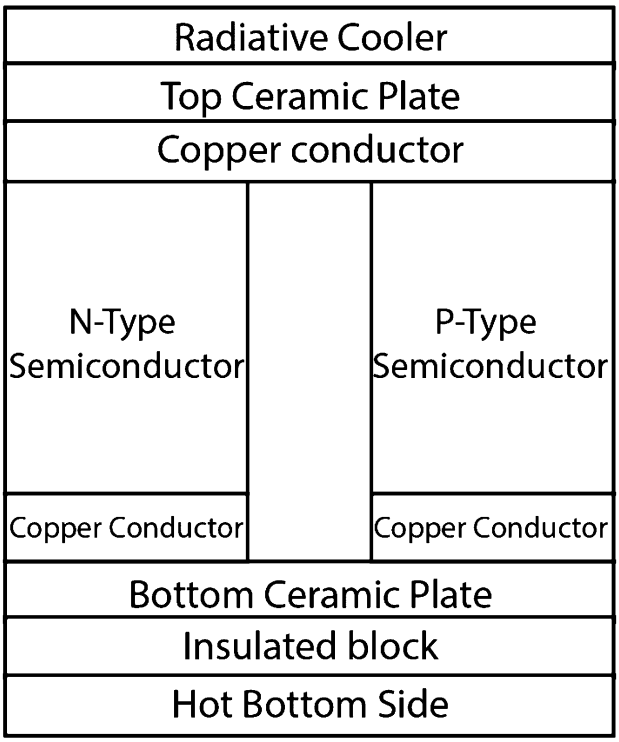

Fig. 4 Thermal model for unit thermocouple representing, (**a**) Thermocouple's different parts (**b**) Thermal resistive circuit ▶

different values of grid sizes. In physics-controlled meshing, the voltage was not balanced, requiring a shift from physics-controlled to user-controlled meshing. In user-controlled meshing, upon iteratively changing the minimum element size, maximum element size, and maximum element growth, a balance in voltage was achieved for all the three plate thickness models at a minimum element size of 0.000008 m, maximum element size of 0.0008 m and a maximum element growth of 1.20.

The number of elements at the mesh independent condition for a model with a plate thickness of 10 mm were 34,935,598 and the study's solution time was 1,034 s. For plate thickness of 5 mm, the number of domain elements were 24,024,473 and solution study time was 687 s and for plate thickness of 2 mm, the number of domain elements were 17,643,662 and solution study time was 337 s. Moreover, mesh independence for the three different cases with respect to maximum elemental growth is also shown in Fig. 5.

6 Experimental setup

The experimental setup used in the present study consisted of two aluminium plates. One of the plates was painted black with commercial black paint as shown in Fig. 7a. This black-painted plate was to behave as a blackbody with an emissivity of 0.95. The other plate was also an aluminium plate but was not painted, as shown in Fig. 7b. The TEG used in the present study was a TEC 12706 with a Seebeck coefficient of 43.5 mV/K which is calculated using Eq. (11) [35].

$$\alpha = \frac{V_{max}}{T_h}, \tag{11}$$

where V_{max} and T_h were obtained from [36]. The hot side of TEC 12706 was coupled with an aluminium block having dimensions of 45 mm × 45 mm and a height of 40 mm, while the cold side was joined with a black painted aluminium plate. Moreover, the bottom surface of the aluminium block was coupled with the normal aluminium plate. The aluminium block was enclosed in polystyrene and polystyrene was covered with aluminium foil to provide as much insulation to the block as possible to constrict the amount of heat flowing out of the block as a result of conduction from a hot aluminium plate. The temperature differential between the top (cold emitter surface) and bottom (hot conductive surface) was measured with K-type thermocouples connected with a K-type thermometer, while the voltage was measured using a digital multimetre. The entire setup was placed on a steel frame whose height was 0.3 m from the rooftop as shown in Fig. 8.

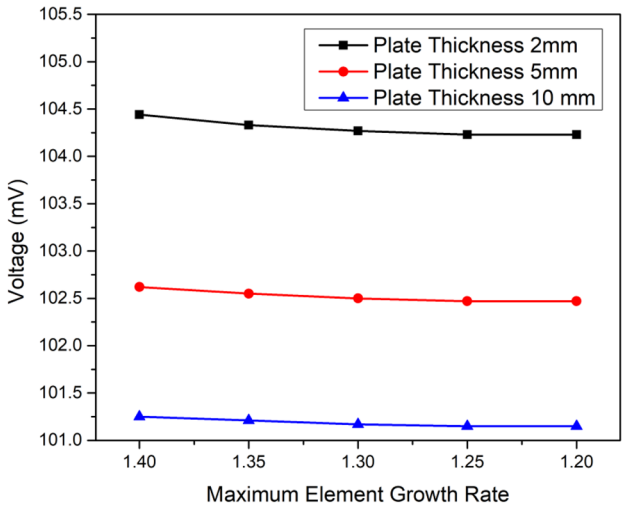

Fig. 5 Mesh independence for three different thicknesses of plates

7 Results and discussion

In the present study, the numerical results were validated by the experimental outcomes. During the experiment, the geometric and operating characteristics were maintained the same. In addition, the numerical study of the parametric influence on the night-time TEG model was also examined. At a temperature difference of 2.5 K, a maximum open-circuit voltage of 92.95 mV was achieved for TEC 12706. Under the same operating conditions, an open-circuit voltage of 104.44 mV was obtained, thereby resulting in an increase

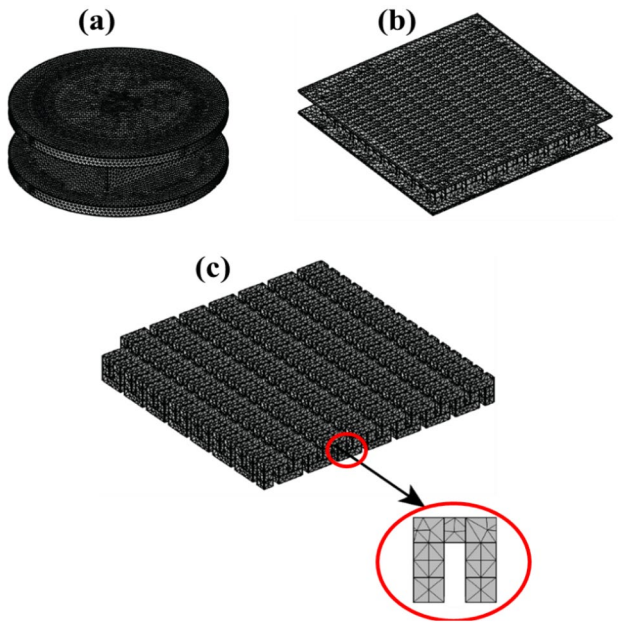

Fig. 6 Mesh representation in (**a**) night-time TEG model (**b**) TEG (**c**) thermopile inside a TEG

Table 3 Grid independence point for a model with 10-mm plate thickness

Min Element Size (m)	Maximum element growth rate	Max Element Size (m)	Domain Elements	Solution study time (s)
8.00E-04	1.4	0.011	132502	30
3.00E-04	1.35	0.007	382827	36
4.00E-05	1.3	0.004	637085	47
1.00E-05	1.25	0.001	18137855	437
8.00E-06	1.2	0.0008	34935598	1034

of 11.49 mV as shown in Fig. 9. This rise might be attributed to the fact that the experimental findings depict the real-world behavior and may include losses such as ohmic, geometric and material concentration losses that were not addressed during the simulation studies. The numerical model's material characteristics may differ from the TEG's real properties [37]. Additionally, convective, radiative, and conductive losses are some of the additional losses in a real TEG. [38].

In a simulation, the ground boundary condition was assigned to the bottom left end of the TEG in Fig. 9a. Thus, voltage generation began there and ended on the bottom right, as shown in Fig. 9a, because the voltage adds up in a series combination, increasing from the first thermocouple on the bottom left to the last thermocouple on the bottom right of Fig. 9a. Furthermore, to study the effect of thickness, the material of the plates, the number of thermocouples, and the height of the thermocouples on the performance of night-time TEG; numerical simulations were performed through parametric assessment. The considered thicknesses were 2, 5, and 10 mm with varying temperature differences. The results are reported in the following sections in terms of the open-circuit voltage, the temperature of the hot surface T_h, the temperature of the cold surface T_c and the time t.

7.1 Effect of change in thickness of the plates

In the first arrangement, the assessment was conducted by assigning the aluminium as the material of the top plate, the bottom plate, and the block. In this arrangement, simulations were performed for three different plate thicknesses. The maximum values of open-circuit voltage obtained were 101.25, 102.62, and 104.44 mV at a temperature difference of 2.5 K for plate thicknesses of 10, 5, and 2 mm, respectively, as shown in Fig. 10. It clearly shows that open-circuit voltage obtained from the numerical simulations was higher than that obtained from experimental results. Moreover, the increase in temperature difference between the plates, increased the corresponding

Table 4 Grid independence point for a model with 5-mm plate thickness

Min Element Size (m)	Maximum element growth rate	Max Element Size (m)	Domain Elements	Solution study time (s)
8.00E-04	1.4	0.011	127154	24
3.00E-04	1.35	0.007	354669	31
4.00E-05	1.3	0.004	545294	51
1.00E-05	1.25	0.001	12585059	340
8.00E-06	1.2	0.0008	24024473	687

Table 5 Grid independence point for a model with 2-mm plate thickness

Min Element Size (m)	Maximum element growth rate	Max Element Size (m)	Domain Elements	Solution study time (s)
8.00E-04	1.4	0.011	117416	23
3.00E-04	1.35	0.007	340541	29
4.00E-05	1.3	0.004	497081	50
1.00E-05	1.25	0.001	11472000	319
8.00E-06	1.2	0.0008	17643662	337

voltage. Furthermore, the results obtained from the simulated open-circuit voltage are near the theoretical results because the voltage generation in thermoelectric materials follow the Eq. (12).

$$\Delta V = \alpha \Delta T, \tag{12}$$

where α represents the Seebeck coefficient, and ΔT is the temperature difference. Taking the Seebeck coefficient of 43.5 mV/K, the theoretical value of the voltage at a temperature difference of 2.5 K is 108.75 mV, and the values obtained from the numerical simulation at the same temperature difference were 101.25, 102.65, and 104.44 mV for the aluminium plates of 10, 5 and 2 mm thicknesses, respectively. Moreover, Eq. (2) clearly shows that the decrease in thickness of bottom plate from which the heat had to move to the bottom of the TEG resulted in an increase of the rate of heat transfer. In addition, a higher temperature difference was obtained across the TEG thereby yielding higher open-circuit voltage. Figure 10 also shows that the voltage fluctuated with time, due to the change in wind velocity. As the wind speed rose, more air particles came into contact with the hot conductive plate, resulting in an increased temperature differential, and vice versa. Similarly, Fig. 11 shows the different values of open-circuit voltage with respect to different temperature differences in increasing order. It can be observed that open-circuit voltage increased with temperature difference. This result is based on the Seebeck phenomenon according to which when two conductors of dissimilar materials are joined together at their ends and then heated, they produce an electric potential. Thus, greater the temperature difference, the greater will be the open-circuit voltage.

7.2 Effect of change in material of the plates

In the second configuration, the impact of the change in plate material was investigated numerically. Copper was chosen as a plate material because it has superior heat conductivity over aluminium. Using the same difference in temperature as in Sect. 7.1, the same three degrees of thickness were tested. The open-circuit voltage at a maximum temperature difference of 2.5 K was 102.24, 103.46, and 105.507 mV for the plate thicknesses of 10, 5, and 2 mm, respectively as shown in Figs. 12 and 13. Moreover, the results indicate that when the material of the plates was changed from aluminium to copper, the open-circuit voltage increased for all three cases of thicknesses, because the Fourier's law of heat conduction (Eq. (2)), clearly shows that higher the thermal conductivity, higher will be the rate of heat transfer. Thus, due to the higher thermal conductivity of copper than aluminium, a high temperature difference was achieved between the top and bottom surfaces of the TEG. Hence, a high open-circuit voltage was achieved as shown in Fig. 12 and 13. Furthermore, Figs. 12 and 13 shows that open-circuit voltage

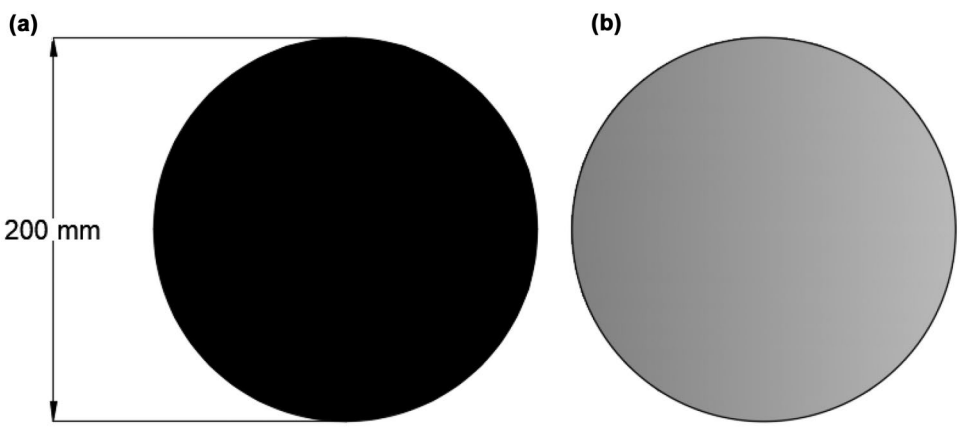

Fig. 7 Aluminium plates (**a**) black painted acting as a thermal emitter, (**b**) non-painted acting as thermal absorber

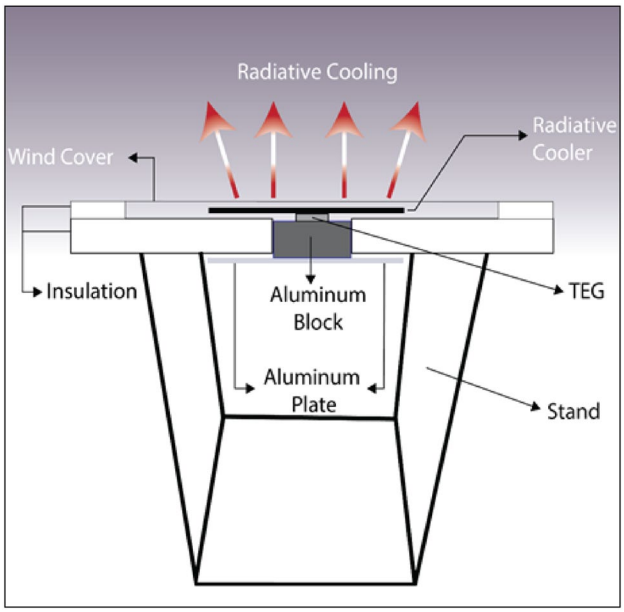

Fig. 8 Night-time TEG experimental setup used in the present study

increased with a decrease of the plate thickness. Moreover, open-circuit voltages obtained using copper as the plates' material was higher than those obtained from aluminium at all the temperatures considered in the present study.

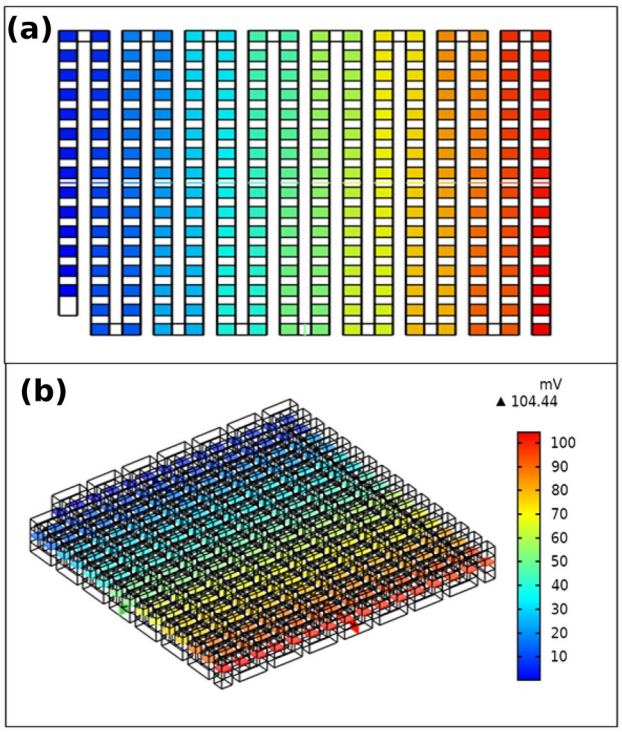

Fig. 9 Voltage distribution in TEG (**a**) two-dimensional representation (**b**) three dimensional

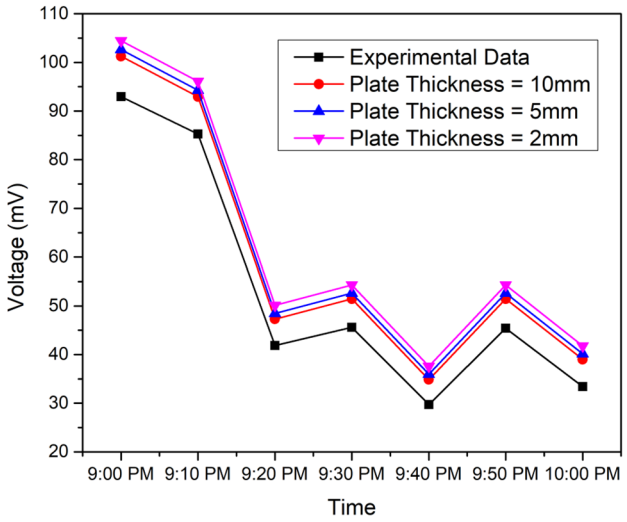

Fig. 10 Comparison of an experimental and numerical model for voltages for different thicknesses of aluminium plates

7.3 Effect of increase in number of thermocouples

The TEG is a combination of a several thermocouples or thermopiles that are temperature-dependent entities capable of producing a voltage in response to the applied temperature gradient and are arranged in series in the TEG to provide the summed-up voltage. Hence, the response of varying the number of thermocouples on the night-time TEG model was also investigated. Thus, the number of thermocouples in the TEG with aluminium plates of 2 mm thickness were increased from 127 to 136 in the simulations. The open-circuit voltage at different temperature differences as

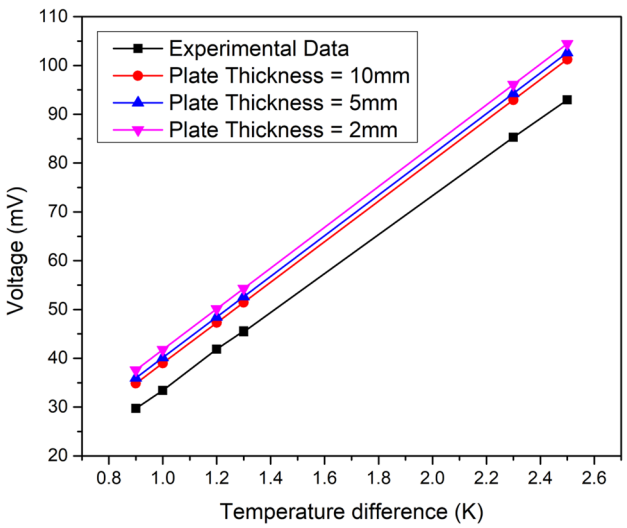

Fig. 11 Effect of aluminium plate thicknesses on voltage vs temperature difference

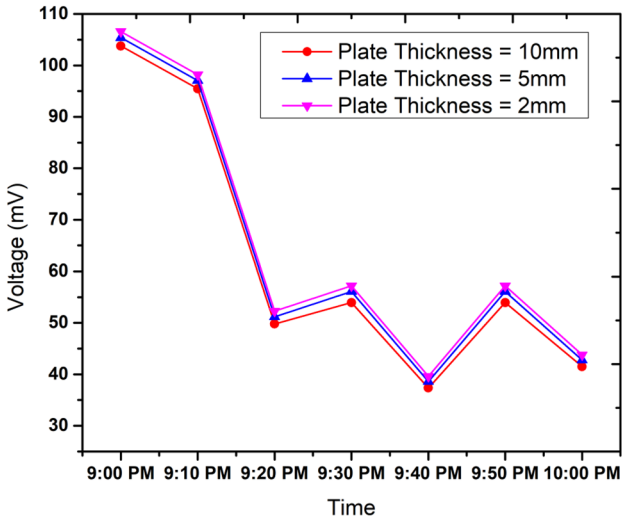

Fig. 12 Numerical prediction of voltage for different thickness of copper plates

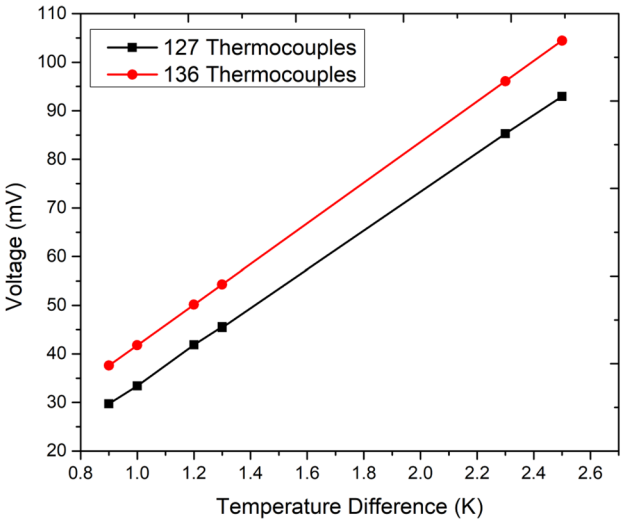

Fig. 14 Effect of increase in thermocouples on the open-circuit voltage at different temperatures

presented in Fig. 14 was higher than the similar night-time TEG model with 127 thermocouples. The finding can be attributed to the equation of the Seebeck effect which obviously indicates that the open-circuit voltage varies directly with the number of thermocouples, the Seebeck coefficient, and the temperature difference between the top and bottom surfaces of the TEG. In this case, the temperature difference and the Seebeck coefficient were the same as those of the 2 mm thick aluminium plates. Thus, a maximum open-circuit voltage for the different temperature values represented in Fig. 14 are obtained as 112.74, 103.72, 58.62, 54.112, and 45.093 mV.

7.4 Effect of increase in leg height of TEG

The influence of modification in the height of the thermocouple's leg was also studied numerically. The height of TEC1-12706 is given in Table 1 to be 1 mm, so it was changed from 1 mm to 1.17 mm, and the impact of the change in height on the open-circuit voltage value was analyzed. The results indicated that increasing the leg height increased the open-circuit voltage. The comparison was performed between thermocouple leg heights of 1 and 1.17 mm for a model with a 10 mm thick aluminium plate. An increase in the value of open-circuit voltage was observed,

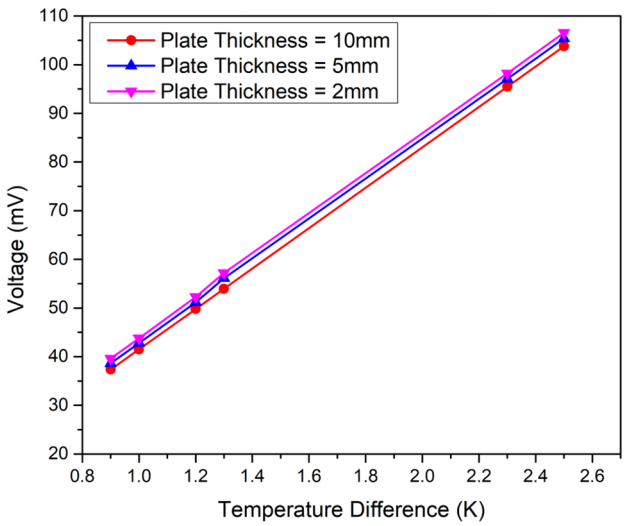

Fig. 13 Numerical prediction of the effect of copper plate thicknesses on voltage vs temperature difference

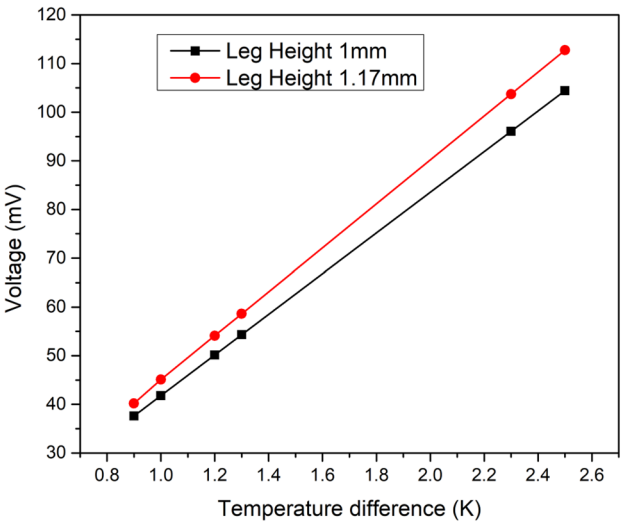

Fig. 15 Impact of leg height on open-circuit voltage for different temperatures

as depicted in Fig. 15. The open-circuit voltage increased because the number of charge carriers (electrons and holes) responsible for conduction increased when the height of P-type and N-Ttype legs increased.

8 Conclusions

In the present study, experimentation and numerical simulations for night-time electricity generation were performed. Results were obtained for the thickness change, the material change, varying the number of thermocouples, and increasing the height of legs of the thermocouple legs. The maximum open-circuit voltage obtained for all the four cases was higher than those with the experimental values. Moreover, it was observed that.

- On reducing the thickness of the top and the bottom plates, the open-circuit voltage increased.
- On changing the material of the top and bottom plates from aluminium to copper, the open-circuit voltage increased.
- On increasing the number of thermocouples, an increase in open-circuit voltage was observed.
- On increasing the height of the TEG legs, an increase in open-circuit voltage was observed.

Hence, as the temperature difference between the top and bottom plates increased, the temperature gradient available across the TEG also increased, consequently the value of open-circuit voltage increased. Moreover, material change from aluminium to copper, the thickness reduction, the increase in the number of thermocouples, and the increase in the height of thermocouples legs increased the open-circuit voltage.

Acknowledgements The authors acknowledge the support of the Interdisciplinary Engineering, Modelling and Simulation Research Group (IEMSRG) of Ghulam Ishaq Khan Institute of Engineering Sciences and Technology, Topi, 23460, KPK, Pakistan.

Funding This study was also supported by a National Research Foundation of Korea (NRF) grant funded by the Korean government (MSIP) (No. 2020R1A2B5B02002512).

Declarations

Conflict of interest All authors declare no conflict of interest of any kind involved with this submission.

References

1. Raman AP, Li W, Fan S (2019) Generating Light from Darkness. Joule 3:2679–2986
2. Cabraal RA, Barnes D, Agarwal SG (2005) Productive uses of energy for rural development. Ann Rev 30:117–144
3. Chu S, Cui Y, Liu N (2016) The path towards sustainable energy. Nat Mater 16:16–22
4. Shindell D, Smith CJ (2019) Climate and air-quality benefits of a realistic phase-out of fossil fuels. Nature 573:408–411
5. Hsu WC, Tong JK, Liao B, Huang Y, Boriskina SV, Chen G (2016) Entropic and near-field improvements of thermoradiative cells. Sci Rep 6:34837
6. Lee K, Correia AJ (2010) A pilot study for investigation of novel methods to harvest solar energy from asphalt pavements. Korea Institute of Construction Technology (KICT), Goyang City, South Korea
7. Fthenakis V, Kim HC (2009) Land use and electricity generation: A life-cycle analysis. Renew Sustain Energy Rev 13:1465–1474
8. Pacca S, Horvath A (2002) Greenhouse gas emissions from building and operating electric power plants in the upper Colorado river basin. Environ Sci Technol 36:3194–3200
9. Yildiz F, Coogler KL (2017) Low power energy harvesting with a thermoelectric generator through an air conditioning condenser. J Eng Technol 34:8–16
10. Zhang Z, Zhang X, Rasim Y, Wang C, Du B, Yuan Y (2016) Design modelling and practical tests on a high-voltage kinetic energy harvesting (EH) system for a renewable road tunnel based on linear alternators. Appl Energy 164:152–161
11. Polman A, Knight M, Garnett EC, Ehrler B, Sinke WC (2016) Photovoltaic materials: Present efficiencies and future challenges. Science 352:4424
12. Lewis NS (2016) Research opportunities to advance solar energy utilization. Science 351:6271
13. Fan L, Li W, Jin W, Orestein M, Fan S (2020) Maximal nighttime electrical power generation via optimal radiative cooling. Opt Express 28:25460–25470
14. Sen R, Bhattacharyya SC (2014) Off-grid electricity generation with renewable energy technologies in India: An application of HOMER. Renew Energy 62:388–398
15. Liu J, Tang H, Zhang D, Jiao S, Zhou Z, Zhang Z, Ling J, Zuo J (2020) Performance evaluation of the hybrid photovoltaic-thermoelectric system with light and heat management. Energy 211:118618
16. Adroja N, Mehta SB, Shah P (2015) Review of thermoelectricity to improve energy quality. J Emerg Technol Innov Res 2:2349–5162
17. Goldsmith HJ (2010) Introduction to Thermoelectricity. Springer, Berlin Heidelberg, p 121
18. Hasebe M, Kamikawa Y, Meiarashi S (2006) Thermoelectric generators using solar thermal energy in heated road pavement. International Conference on Thermoelectrics ICT. IEEE, Vienna, pp 697–700
19. Guangxi W, Xiong Y (2012) Thermal Energy Harvesting Across Pavement Structure. Transportation Research Board 91st Annual Meeting, Washington DC, United States. 22-26 January, 2012
20. Datta U, Dessouky S, Papagiannakis AT (2017) Harvesting Thermoelectric Energy from Asphalt Pavements. Trans Res Rec 2628:12–22
21. Zhan Z, ElKabbash M, Li Z, Li X, Zhang J, Rutledge J, Singh S, Guo C (2019) Enhancing thermoelectric output power via radiative cooling with nanoporous alumina. Nano Energy 65:104060
22. Zhao B, Pei G, Raman AP (2020) Modeling and optimization of radiative cooling based thermoelectric generators. Appl Phys 117:163903
23. Zhou Z, Wang Z, Bermel P (2019) Radiative cooling for low-bandgap photovoltaics under concentrated sunlight. Opt Express 27:A404–A418
24. Fan S (2017) Thermal Photonics and Energy Applications. Joule 1:264–273

25. Leblanc S (2014) Thermoelectric generators: Linking material properties and systems engineering for waste heat recovery applications. Sustain Mater Technol 1:26–35
26. Zhao D, Aili A, Zhai Y, Xu S, Tan G, Yin X, Yang R (2019) Radiative sky cooling: Fundamental principles, materials, and applications. Appl Phys Rev 6:021306
27. Lim XZ (2020) The super-cool materials that send heat to space. Nature 577:18–20
28. Santhanam P, Fan S (2016) Thermal-to-electrical energy conversion by diodes under negative illumination. Phys Rev B 93:16140
29. Berdahl P (1985) Radiant refrigeration by semiconductor diodes. J Appl Phys 58:1369–1374
30. Buddhiraju S, Santhanam P, Fan S (2018) Thermodynamic limits of energy harvesting from outgoing thermal radiation. Proc Natl Acad Sci USA 115:3609–3615
31. Byrnes SJ, Blanchard R, Capasso F (2014) Harvesting renewable energy from Earth's mid-infrared emissions. Proc Natl Acad Sci USA 111:3927–3932
32. Raman AP, Anoma MA, Zhu L, Rephaeli E, Fan S (2014) Passive radiative cooling below ambient air temperature under direct sunlight. Nature 515:540–544
33. Zhai Y, Ma Y, David SN, Zhao D, Lou R, Tan G, Yin X (2017) Scalable-manufactured randomized glass-polymer hybrid metamaterial for daytime radiative cooling. Science 355:1062–1066
34. Ishii S, Dao TD, Nagao T (2020) Radiative cooling for continuous thermoelectric power generation in day and night Radiative cooling for continuous thermoelectric power generation in day and night. Appl Phys 117:013901
35. Shen L, Chen H, Xiao F, Wang S (2015) The practical performance forecast and analysis of thermoelectric module from macro to micro. Energy Convers Manag 100:23–29
36. http://www.highpurity-metals.com/sale-10192413-bite-material-thermoelectric-cooler-peltier-tec-module-60w-for-cooling-tec-12706.html
37. Lee H, Shar J, Stokes D, Pearson M, Priya S (2018) Modeling and analysis of the effect of thermal losses on thermoelectric generator performance using effective properties. Appl Energy 211:987–996
38. Bjørk R, Christensen DV, Eriksen D, Pryds N (2014) Analysis of the internal heat losses in a thermoelectric generator. Int J Therm Sci 85:12–20